



**HAL**  
open science

## Dynamics of dikes versus cone sheets in volcanic systems

Olivier Galland, Steffi Burchardt, Erwan Hallot, Régis Mourgues, Cédric  
Bulois

► **To cite this version:**

Olivier Galland, Steffi Burchardt, Erwan Hallot, Régis Mourgues, Cédric Bulois. Dynamics of dikes versus cone sheets in volcanic systems. *Journal of Geophysical Research*, 2014, 119 (8), pp.6178-6192. 10.1002/2014JB011059 . insu-01064709

**HAL Id: insu-01064709**

**<https://insu.hal.science/insu-01064709>**

Submitted on 17 Sep 2014

**HAL** is a multi-disciplinary open access archive for the deposit and dissemination of scientific research documents, whether they are published or not. The documents may come from teaching and research institutions in France or abroad, or from public or private research centers.

L'archive ouverte pluridisciplinaire **HAL**, est destinée au dépôt et à la diffusion de documents scientifiques de niveau recherche, publiés ou non, émanant des établissements d'enseignement et de recherche français ou étrangers, des laboratoires publics ou privés.

## RESEARCH ARTICLE

10.1002/2014JB011059

## Key Points:

- Dynamic laboratory models simulate dikes (D) and cone sheets (CS)
- D and CS correspond to two physical regimes of magma emplacement in the Earth's crust
- The sharp transition between the D and CS regimes governed by a power law

## Correspondence to:

O. Galland,  
olivier.galland@fys.uio.no

## Citation:

Galland, O., S. Burchardt, E. Hallot, R. Mourgues, and C. Bulois (2014), Dynamics of dikes versus cone sheets in volcanic systems, *J. Geophys. Res. Solid Earth*, 119, doi:10.1002/2014JB011059.

Received 20 FEB 2014

Accepted 8 JUL 2014

Accepted article online 17 JUL 2014

## Dynamics of dikes versus cone sheets in volcanic systems

Olivier Galland<sup>1</sup>, Steffi Burchardt<sup>2</sup>, Erwan Hallot<sup>3</sup>, Régis Mourgues<sup>4</sup>, and Cédric Bulois<sup>4</sup>

<sup>1</sup>Physics of Geological Processes, Department of Geosciences, University of Oslo, Oslo, Norway, <sup>2</sup>Solid Earth Geology, Department of Earth Sciences, Uppsala University, Uppsala, Sweden, <sup>3</sup>Géosciences Rennes, UMR CNRS 6118, OSUR, Université de Rennes, Rennes, France, <sup>4</sup>L.P.G.N., UMR CNRS 6112, Faculté des Sciences, Université du Maine, Le Mans, France

**Abstract** Igneous sheet intrusions of various shapes, such as dikes and cone sheets, coexist as parts of complex volcanic plumbing systems likely fed by common sources. How they form is fundamental regarding volcanic hazards, yet no dynamic model simulates and predicts satisfactorily their diversity. Here we present scaled laboratory experiments that reproduced dikes and cone sheets under controlled conditions. Our models show that their formation is governed by a dimensionless ratio ( $\Pi_1$ ), which describes the geometry of the magma source, and a dynamic dimensionless ratio ( $\Pi_2$ ), which compares the viscous stresses in the flowing magma to the host rock strength. Plotting our experiments against these two numbers results in a phase diagram evidencing a dike and a cone sheet field, separated by a sharp transition that fits a power law. This result shows that dikes and cone sheets correspond to distinct physical regimes of magma emplacement in the crust. For a given host rock strength, cone sheets preferentially form when the source is shallow, relative to its lateral extent, or when the magma influx velocity (or viscosity) is high. Conversely, dikes form when the source is deep compared to its size, or when magma influx rate (or viscosity) is low. Both dikes and cone sheets may form from the same source, the shift from one regime to the other being then controlled by magma dynamics, i.e., different values of  $\Pi_2$ . The extrapolated empirical dike-to-cone sheet transition is in good agreement with the occurrence of dikes and cone sheets in various natural volcanic settings.

### 1. Introduction

Swarms of igneous sheet intrusions represent the main magma pathways through the Earth's brittle crust. They form substantial volumes of long-lived volcanic edifices [Walker, 1992] and correspond to the main feeders of volcanic eruptions in basaltic and andesitic volcanoes [e.g., Amelung et al., 2000; Sigmundsson et al., 2010; Chadwick et al., 2011] (Figure 1). Field observations in extinct and exhumed volcanic areas worldwide have identified different geometries of sheet intrusions, among which (i) vertical dikes [e.g., Pollard, 1987; Lister and Kerr, 1991; Rubin, 1995; Ancochea et al., 2003; Geshi, 2005; Paquet et al., 2007], (ii) inclined cone sheets [Harker and Clough, 1904; Bailey, 1924; Ancochea et al., 2003; Burchardt et al., 2011], and (iii) horizontal sills [e.g., Kavanagh et al., 2006; Burchardt, 2008; Galland et al., 2009] represent the main types (Figure 1). It is interesting to notice that although the shapes of these distinct sheet intrusions are rather different, they are found together in the same volcanic systems (Figure 1) [Walker, 1992; Geshi, 2005; Paquet et al., 2007] and their thicknesses follow the same statistical distribution indicating a related emplacement dynamics [Krumbholz et al., 2014]. The spatial association and the close temporal relations between cone sheets and dikes led Walker [1992] to propose that they may be fed by a common source [see also Geshi, 2005]. The following key question, however, remains unsolved: what are the physical parameters that lead either to vertical dikes or cone sheets in volcanic systems, and particularly those fed from the same source?

The mechanisms of cone sheet and dike emplacement have been studied for decades [e.g., Anderson, 1936; Phillips, 1974; Chadwick and Dieterich, 1995; Bistacchi et al., 2012; Chestler and Grosfils, 2013]. Most models address these emplacement processes through semistatic conditions and are usually based on the assumption of purely elastic host rocks. The procedure is the following: (i) a magma reservoir of given size and shape is overpressurized; (ii) the resulting elastic stress field is calculated in the host rock; (iii) the pressure in the reservoir is increased until the stresses at the reservoir wall reach the strength of the host rock; and (iv) then, at failure, the orientation of the principal stresses in the host rock is interpreted as favoring the formation of either dikes or cone sheets. Although useful to provide a first-order understanding, such models do not simulate the dynamics of dike or cone sheet emplacement, the occurrence of which is indirectly inferred

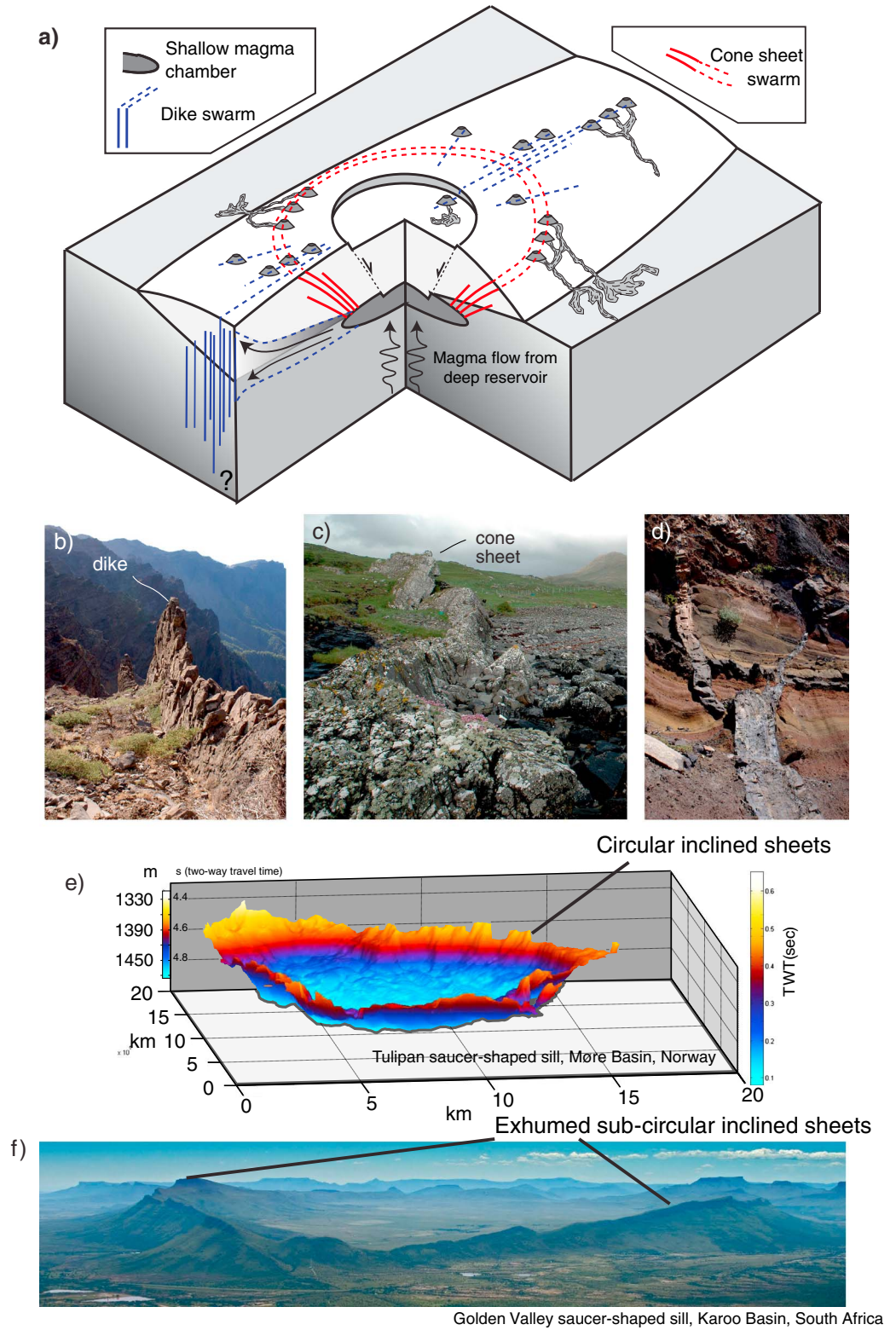


Figure 1

from stress calculations within the host rock. In addition, these models account neither for magma dynamics, e.g., viscosity effects, nor the plastic rheology of natural host rocks, indicating that our general understanding of the mechanics of magma intrusion into the crust is still rather weak.

Sheet intrusions observed in distinct volcanic settings exhibit strikingly similar features. Good examples are cone sheets in central volcanoes and saucer-shaped sills in sedimentary basins. Cone sheets consist of subcircular inward dipping sheets, fed from a magma reservoir [Schirnick *et al.*, 1999; Klausen, 2004; Burchardt *et al.*, 2011], while saucer-shaped sills also exhibit subcircular inward dipping inclined sheets, fed by a horizontal sill (Figures 1e and 1f) [Malthe-Sørenssen *et al.*, 2004; Galland *et al.*, 2009; Galerne *et al.*, 2011; Galland and Scheibert, 2013]. Both types of intrusions are assumed to form when the magma feeder source (a magma reservoir or a flat horizontal sill) interacts with the deformable free surface. Despite their similarities, their emplacement mechanisms are generally addressed through distinct models, and a single general mechanical model bridging cone sheets and saucer-shaped sills is lacking.

Geological observations show that both dikes and cone sheets have successively built complex plumbing systems that are a combination of both intrusion types (La Gomera, Canary Islands [Ancochea *et al.*, 2003] and Otoge igneous complex, Central Japan [Geshi, 2005]); these two types of intrusions might have fed radial and circumferential eruptive fissures, respectively. The reason why dikes alternate with cone sheets in these complexes is poorly understood. Geshi [2005] proposes that the emplacement of dikes and cone sheets at the Otoge igneous complex resulted from varying magma influx rate into the reservoir. Ancochea *et al.* [2014] describe a phonolitic cone sheet swarm intimately associated to a radial basaltic dike swarm from Cape Verde, Central Atlantic, which suggests that magma viscosity might also control the occurrence of dikes or cone sheets. These inferences show that a mechanical model predicting under which conditions dikes and cone sheets form is needed for improving volcanic hazards assessment in these volcanoes, given that the location of eruptive vents associated with dikes or cone sheets are rather different (Figure 1a).

The only dynamic models simulating both dikes and cone sheets are laboratory models [McLeod and Tait, 1999; Mathieu *et al.*, 2008; Galland *et al.*, 2009; Abdelmalak *et al.*, 2012; Galland, 2012]. Although these models manage to reproduce both types of sheet intrusions, they do not provide the mechanical laws governing the formation of dikes or cone sheets, because no systematic parameter study has been conducted. In this paper, we present a quantitative parameter study based on 51 experiments that simulate dikes and cone sheets. Combined with a dimensional analysis of the mechanical problem, we show that dikes and cone sheets correspond to two distinct mechanical regimes of magma emplacement.

## 2. Experimental Method

To study the dynamics of dike and cone sheet formation, we performed laboratory experiments scaled to simulate the intrusion of a low-viscosity magma into the brittle upper crust. The crystalline silica flour, which was used in the experiments to simulate the brittle crust, is produced by Sibelco, in Belgium, and sold under the name M400, with an average grain size of  $\sim 15 \mu\text{m}$ . It was compacted using a high-frequency compressed-air shaker (Houston Vibrator, model GT-25), following a procedure that achieves homogeneous, repeatable, and fast compactations [Galland *et al.*, 2009; Galland, 2012; Galland *et al.*, 2014a]. The flour fails according to a Mohr-Coulomb criterion, and we measured the cohesion ( $C$ ) and friction coefficient ( $\mu$ ) of compacted flour to be  $369 \pm 44 \text{ Pa}$  and  $0.81 \pm 0.06$ , respectively [Galland *et al.*, 2009], using a Hubbert shear box, as described by Hubbert [1951] and Mourgues and Cobbold [2003]. This value is, within errors, the same as that measured by Galland *et al.* [2006], who also measured the tensile strength  $T \sim 100 \text{ Pa}$ . The density of the silica flour is

**Figure 1.** (a) Schematic drawing of the characteristic structure of volcano plumbing systems. A shallow magma reservoir may feed different conduits, such as dikes (blue) or cone sheets (red). Drainage of the shallow reservoir may also lead to the formation of a caldera. Some of the dikes and cone sheets may result in eruptive fissures, the locations of which depend on the geometry of the conduit breaching the surface. Note that dikes are often oriented along rift zones, controlling elongated shapes of volcanic edifices. (b–d) Field photographs of exposed magma conduits of various shapes: a dike in the Taburiente shield volcano, La Palma, Canary Islands, a cone sheet in the Ardnamurchan volcanic complex, Scotland, and a dike tip splitting up into two branches in Taburiente volcano, respectively. (e) Three-dimensional geometry of a saucer-shaped sill from the Tulipan sill, Møre Basin offshore Norway, reconstructed from 3-D seismic data [Polteau *et al.*, 2008b; Galland *et al.*, 2009]. Similar to cone sheets, it exhibits subcircular inward dipping inclined sheets. (f) Aerial photograph of the exhumed Golden Valley saucer-shaped sill, Karoo Basin, South Africa [Polteau *et al.*, 2008a; Polteau *et al.*, 2008b]. The prominent ridges correspond to elliptical, inward dipping inclined sheets fed from flat inner sill [Galerie *et al.*, 2011].

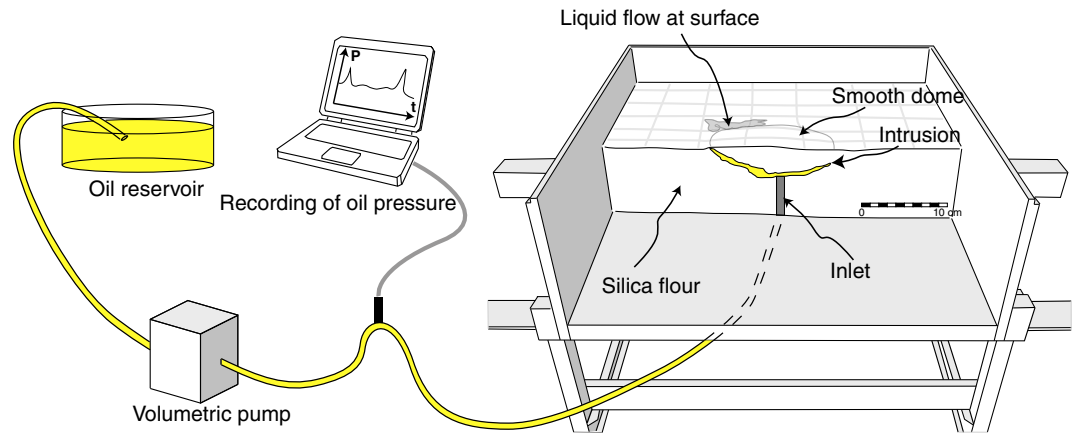


**Figure 2.** Drawing of the experimental apparatus used in this study.

1050 kg m<sup>-3</sup> when compacted. Measurements also yielded an angle of internal friction of  $\Phi \sim 39^\circ$ , calculated from the friction coefficient measured by Galland *et al.* [2009].

The vegetable oil, simulating the magma, is produced by Unilever and sold in France under the name Végétaline. It is solid at room temperature but melts at  $\sim 31^\circ\text{C}$ . The viscosity of the oil is poorly temperature dependant [Galland *et al.*, 2006]; we injected it at  $\sim 50^\circ\text{C}$ , at which its viscosity is  $\eta \sim 2 \times 10^{-2}$  Pa s and density is  $890 \text{ kg m}^{-3}$ .

The experimental apparatus used in this study is a modified version of that of Galland *et al.* [2009] and Galland [2012]. The models were performed in a 40 cm wide square box filled with a layer of compacted silica flour of variable thickness and controlled density of  $1050 \text{ kg m}^{-3}$  (Figure 2). Initial layer surfaces were flat. A pump injected the oil at constant and controlled flow rate through a circular inlet of variable diameter ( $d = 2, 5,$  or  $10 \text{ mm}$ ), and the oil intruded directly into the silica flour. The average oil velocity at the outlet, or oil injection velocity ( $v$ ), was calculated by dividing the pump volumetric flow rate by the section area of the injection inlet pipe. Oil intrusion triggered deformation of the surface of the models, producing a smoothly varying relief above the intrusion [Galland, 2012]. The experimental apparatus does not simulate regional deformation, and neither layering nor localized heterogeneities in the crust were taken into account. In addition, cooling effects of the oil were negligible for the duration of an experiment [Galland *et al.*, 2006].

We present the results of 51 experiments, in which we varied independently three controlled parameters: the depth of the injection inlet ( $h$ ) below the free surface, the diameter of the injection inlet ( $d$ ), and the oil injection velocity ( $v$ ). The ranges of the experimental parameters that we explored are listed in Table 1. Each

<b>Table 1.</b> List of Parameters Used in This Study and Their Values in Experiments and Different Geological Settings <sup>a</sup>				
Values	Experiments	Magma Reservoirs	Sills	Dike Tips
$h$ (m)	0.02–0.1	2,000–15,000	500–5,000	10–10,000
$d$ (m)	0.002–0.01	1,000–50,000	1,000–50,000	0.1–1
$w$ (m)	–	1,000–3,000	50–200	–
$\rho_r$ (kg m <sup>-3</sup> )	1050	2,500	2,500	2,500
$\rho_m$ (kg m <sup>-3</sup> )	890	2,500–2,700	2,500–2,700	2,500–2,700
$C$ (Pa)	350	$10^5$ – $10^7$	$10^6$ – $10^7$	$10^6$ – $10^7$
$\phi = \Pi_3$	39	25–45	25–45	25–45
$\eta$ (Pa s)	$2 \times 10^{-2}$	$100$ – $10^7$	$100$ – $10^5$	$100$ – $10^6$
$v$ (m s <sup>-1</sup> )	0.017–0.21	0.0001–0.01	0.005–0.05	0.01–0.1
<i>Magma-Host</i>				
$\Pi_1$	3–30	0.04–15	0.01–1	10–100,000
$\Pi_2$	$9 \times 10^{-5}$ – $5 \times 10^{-3}$	$3.3 \times 10^{-13}$ – $10^{-3}$	$2.5 \times 10^{-10}$ – $10^{-4}$	$10^{-7}$ –1
<i>Magma Flow</i>				
$\Pi_5 = Re$	1.5–94	$2.5 \times 10^{-5}$ –810	0.006–270	$2.5 \times 10^{-6}$ – $6.3 \times 10^{-3}$
<i>Buoyancy</i>				
$\Pi_6$	0.15	–0.08–0	–0.08–0	–0.08–0

<sup>a</sup>Note that when the lateral extent ( $d$ ) of magmatic sources is the same as its thickness ( $w$ ), no value of  $w$  is given.

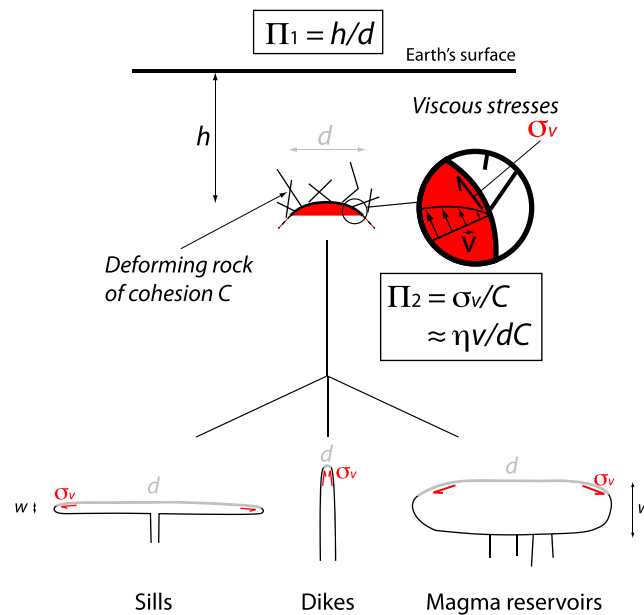


**Figure 3.** Schematic drawing describing the definitions and illustrating the physical meanings of the main dimensionless parameters  $\Pi_1 = h/d$  and  $\Pi_2 = \eta v/dC$  used in this study.

experiment lasted typically for a minute; injection was stopped once the oil erupted at the model surface. After the end of an experiment, the oil solidified after about half an hour, and the intrusions were then exhumed. Excavated intrusions consisted of a main core of pure oil surrounded by a thin rim of mixed oil and flour that resulted from percolation [Galland *et al.*, 2006, 2007]. The experimental protocol used in this study produced repeatable results, as it has been verified from selected experiments that were repeated twice. The consistency of our results (see section 4) confirms a posteriori the repeatability of our protocol. The repeatability of this protocol has also been tested by Galland *et al.* [2009], who repeated twice their whole experimental series and produced rigorously the same results.

### 3. Dimensional Analysis

The aims of the dimensional analysis are to (i) identify the dimensionless parameters governing the modeled processes and (ii) test the similarity of the laboratory models with the geological systems they intend to simulate [Barenblatt, 2003; Galland *et al.*, 2014b]. In models designed for simulating magma emplacement in the brittle crust, the scaling is challenging because (i) natural magma viscosities vary over broad ranges and (ii) both the dynamics within the magma and the deforming country rock should be properly scaled. The principle is to define selected dimensionless numbers, which characterize the geometry, the kinematics, and the kinetics of the simulated processes. The scaling procedure is based on standard similarity conditions as developed by Hubbert [1937], Ramberg [1981], and Barenblatt [2003] and used, for example, by Merle and Borgia [1996] or Galland *et al.* [2014a].

In both our experiments and nature, the principal geometrical input variables are the depth ( $h$ ) of the injection inlet, or the depth of magmatic sources feeding sheet intrusions, the diameter ( $d$ ) of the inlet, or the effective lateral extent of the magmatic sources. Also known, and controlled in the experiments, are the oil/magma injection velocity ( $v$ ), density ( $\rho_m$ ), and viscosity ( $\eta$ ), and the flour/country rock properties, such as density ( $\rho_r$ ), angle of internal friction ( $\Phi$ ), and cohesion ( $C$ ). An external parameter, identical in both systems, is gravity ( $g$ ). As our experiments aimed to simulate volcano- and basin-scale phenomena, we chose a model-to-nature scale ratio between  $10^{-5}$  and  $10^{-4}$ , i.e., 1 cm in experiments represents 1 km to 100 m in nature.

According to the Buckingham-II theorem [Barenblatt, 2003; Galland *et al.*, 2014b], the nine variables from the list above, minus three which have independent dimensions (e.g.,  $h$ ,  $C$ , and  $v$ ), define six independent dimensionless numbers that characterize the physical system. As discussed below and illustrated in Figure 3, two of these dimensionless numbers, a geometrical ratio  $\Pi_1$  and a dynamic ratio  $\Pi_2$ , account for the coupling between the magmatic source and the country rock and appear to exert dominant controls on the formation of sheet intrusions. As we shall discuss and compare the values of these ratios in models and various geological settings, and because a robust estimate of the values of the dimensionless numbers in natural systems is challenging, the following sections only provide rough estimates given as orders of magnitude.

First, let us consider the geometric depth-to-size (lateral extent) ratio of the magma source (Figure 3):

$$\Pi_1 = h/d. \tag{1}$$

In the experiments,  $\Pi_1$  ranges from 3 to 30 (Figure 5 and Table 1). In nature,  $\Pi_1$  covers a very broad range of values depending on the type of magma source (Table 1). Depending on the considered geological systems (e.g., dikes, sills, and magma reservoirs),  $d$  may take very different values. Within volcanoes, magmatic sources of sheet intrusions can be assumed to correspond to the whole or only to the efficient parts of main magma reservoirs. Thus, maximum  $d$  values are given by the diameters of roughly spherical or ellipsoidal reservoirs [Bistacchi *et al.*, 2012]. Conical sheet intrusions also form in many sedimentary basins where they correspond to the inclined sheets of saucer-shaped sills [Malthe-Sørensen *et al.*, 2004; Galland *et al.*, 2009; Galland and Scheibert, 2013]. In such a case, the magmatic sources are flat sills, and  $d$  is given by their diameters. As sill diameters are usually larger than they are deep [Polteau *et al.*, 2008b; Galland *et al.*, 2009], we assume an upper limit case of  $\Pi_1 = 1$  for sills. Finally, seismic observations [Bureau *et al.*, 2013] and laboratory models [Mathieu *et al.*, 2008; Abdelmalak *et al.*, 2012; Galland, 2012; Mourgues *et al.*, 2012] show that dike tips sometimes split into conical sheets, suggesting that dike tips can also be considered as local moving magmatic sources for dikes or cone sheets. In these cases, as the conical sheets are rooted along the walls of the dikes, but not strictly to their tips,  $d$  is expected to be the dike thickness.

The second dimensionless parameter is the dynamic ratio between the viscous stresses due to magma flow and the strength of the country rock. For laminar flow of a Newtonian fluid of viscosity  $\eta$  flowing at a velocity  $v$ , the viscous stresses induced by the flow of magma across a conduit of thickness  $d$  is  $\sigma_v \propto \eta v/d$  assuming a Poiseuille flow (Figure 3). Note that this expression describes a local mechanical coupling between the viscous magma and its host rock, but not the integrated pressure drop along whole length of a dike. Thus, the expression of  $\Pi_2$  is the following:

$$\Pi_2 = \frac{\eta v}{C d}. \quad (2)$$

$\Pi_2$  has the same form as that of the Bingham number, which expresses the ratio between the viscous stress and the yield stress within a single Bingham fluid. The main difference in our system is that  $\Pi_2$  expresses the stress ratio between two different materials. In our experiments, the values of  $\Pi_2$  span between  $9 \times 10^{-5}$  and  $5 \times 10^{-3}$  (Table 1).

To estimate the values of  $\Pi_2$  in geological systems, one needs to keep in mind its physical meaning, i.e., the ratio between the viscous stresses and the strength of the host rock. Calculating the maximum viscous stresses implies that  $d$  corresponds to the minimum size of the zone across which the magma is flowing within the magmatic source. In our experiments, the thickness of the inlet is thus the same as its lateral extent used to calculate  $\Pi_1$ . This is the same for a dike, where  $d$  is the dike thickness. Nevertheless, in magmatic systems like sills or flat-lying magma reservoirs, the thicknesses of the magma sources across which the magma can flow are smaller than their lateral extents. In Table 1, the thickness of the magmatic source, when different from lateral extent, is referred to as  $w$ .

For dikes, considering viscosities between 100 Pa s for basaltic melts and  $10^6$  Pa s for andesite-rhyolite magma [Dingwell *et al.*, 1993],  $\Pi_2$  values range from  $10^{-7}$  to 1 (Table 1). Saucer-shaped sills are usually filled with poorly evolved magmas [Galerne *et al.*, 2008] with viscosities likely ranging from 100 to  $10^5$  Pa s. Thus, the values of  $\Pi_2$  span between  $2.5 \times 10^{-10}$  and  $10^{-4}$  (Table 1). Finally, estimating the values of  $\Pi_2$  for magma reservoirs under volcanoes is challenging as the dynamics of magma accumulation are poorly constrained. Again, considering magma viscosities in the range  $100$ – $10^7$  Pa s, in a typically 1000 m to 3000 m thick flat-lying reservoir, the magma velocities due to thermal convection or magma replenishment can be expected to be between  $10^{-4}$  and  $10^{-2}$  m s $^{-1}$  [Huppert and Sparks, 1981; Sparks *et al.*, 1984]. Considering that the country rocks of magma reservoirs can be weakened due to fracturing and heating, their strengths are expected to be low [Krumbholz *et al.*, 2014] and their cohesion is expected to range from  $10^5$  to  $10^7$  Pa. Thus, the values of  $\Pi_2$  for magma reservoirs under volcanoes are expected to range from  $3 \times 10^{-13}$  to  $10^{-2}$  (Table 1).

Note that our models do not take into account cooling effects, which may induce significant magma viscosity increase. In nature, cooling may affect the value of  $\Pi_2$ .

According to the Buckingham- $\Pi$  theorem [Barenblatt, 2003], four other dimensionless parameters should be discussed. These parameters, however, play a minor role for interpreting our experimental results, as they

**Table 2.** List of Parameters Used to Scale the Properties of the Country Rock

Host	Experiments	Nature
$\Pi_3$	39	25–45
$\Pi_4$	0.6–2.9	0.24–245

account for either the behavior of the country rock ( $\Pi_3$  and  $\Pi_4$ ) or the magma flow ( $\Pi_5$ ), separately. Because  $\Pi_3$  and  $\Pi_4$  only account for the mechanical behavior of the country rock, their values are independent of the intrusion type, and they are quoted in the separate Table 2.

An obvious dimensionless parameter accounting for the brittle behavior of the flour and country rock is the angle of internal friction:

$$\Pi_3 = \phi. \quad (3)$$

The angle of internal friction of the silica flour is about  $39^\circ$ , which is in the range of those of natural rocks, although it is close to its upper bound [Schellart, 2000]. In addition, the natural range of values of  $\Pi_3$  is narrow compared to those of  $\Pi_1$  and  $\Pi_2$ . Therefore,  $\Pi_3$  is not considered further in the analysis.

Another dimensionless number to scale the brittle country rock is the ratio of gravitational stress to cohesion:

$$\Pi_4 = \frac{\rho_r g h}{C}. \quad (4)$$

Here  $h$  is taken as the characteristic scale of the whole system. In our experiments,  $h$  corresponds to the injection depth, and  $\Pi_4$  range from 0.6 to 2.9 (Table 2). In natural systems, typical sizes of volcanic systems are between 1 and 10 km; an average density for natural rocks is about  $2500 \text{ kg m}^{-3}$ , but range from 2300 to  $2900 \text{ kg m}^{-3}$  for sedimentary and magmatic rocks. Their typical cohesion is between  $10^6$  and  $10^7 \text{ Pa}$  [Schellart, 2000]. Thus, overall values of  $\Pi_4$  in nature range from 0.24 to 245. The values of  $\Pi_4$  in the experiments thus overlap those in natural systems at their lower bound, suggesting that the silica flour represents relatively strong rocks.

The dimensionless number that accounts for the flow regime of magma within intrusions (laminar versus turbulent) is the Reynolds number, which is the ratio between inertial and viscous forces:

$$\Pi_5 = Re = \frac{\rho_m d v}{\eta}. \quad (5)$$

In our experiments, the values of  $Re$  range from 1.5 to 94, so that the flow regime of the oil is laminar (Table 1). Similarly to  $\Pi_2$ , here  $d$  denotes the thickness of the magmatic conduit. For the various natural magma conduits considered in this study, the values of  $Re$  span between  $2.5 \times 10^{-6}$  and 810 (Table 1). These values are smaller than most of the critical values of the Reynolds number for turbulence. Thus, magma flow in magma conduits is also mostly laminar. However, in case of very fluid magma flowing at high velocity in thick magma reservoirs, turbulence may occur.

Note that both  $\Pi_4$  and  $\Pi_5$  use the same parameters  $C$ ,  $h$ ,  $v$ ,  $d$ , and  $\eta$  as  $\Pi_1$  and  $\Pi_2$ ; therefore, they are not useful to interpret the results, since the effects of  $C$ ,  $h$ ,  $v$ ,  $d$ , and  $\eta$  are already taken into account using  $\Pi_1$  and  $\Pi_2$ .

The final dimensionless number is the ratio of hydrostatic forces to lithostatic forces, corresponding to the buoyancy of the magma, which can be expressed by the following:

$$\Pi_6 = 1 - \rho_m / \rho_r. \quad (6)$$

When  $\Pi_6 < 0$ , the magma is heavier than the country rock, and negatively buoyant; in contrast, when  $\Pi_6 > 0$ , the magma is lighter than the country rock, the magma is buoyant. In nature, degassed magma densities typically vary between  $\sim 2500$  and  $\sim 2700 \text{ kg m}^{-3}$ , and  $\Pi_6$  ranges from  $-0.08$  to 0 in the upper sedimentary crust, so that magma is dominantly neutrally buoyant to negatively buoyant. In contrast, in our experiments,  $\Pi_6 = 0.15$ , so that the oil is positively buoyant. Such a situation occurs in dense mafic host rocks forming volcanic edifices when light magma can form intrusions near the surface where gas nucleation may substantially decreases melt densities [Menand and Tait, 2001].

In geological systems, the combined effects of magma buoyancy and overpressure govern the velocity of dike propagation [Takada, 1990; Menand and Tait, 2002]. Nevertheless, in our experiments, the velocity is controlled by the volumetric pump. Therefore, controlling the injection flow rate is equivalent to controlling the buoyancy; this dimensionless number is thus not an important parameter of the physical system

**Table 3.** List of Experiments and Experimental Parameters Explored in This Study

Experiment	$h$ (m)	$d$ (m)	$v$ ( $\text{m s}^{-1}$ )	Intrusion
1	0.03	0.01	0.017	CS
2	0.04	0.01	0.017	CS
3	0.06	0.01	0.017	H
4	0.08	0.01	0.017	D
5	0.1	0.01	0.017	D
6	0.02	0.005	0.017	CS
7	0.03	0.005	0.017	CS
8	0.04	0.005	0.017	H
9	0.05	0.005	0.017	D
10	0.03	0.005	0.0255	CS
11	0.04	0.005	0.0255	CS
12	0.05	0.005	0.0255	D
13	0.06	0.005	0.0255	D
14	0.06	0.005	0.0255	D
15	0.02	0.005	0.0339	CS
16	0.03	0.005	0.0339	CS
17	0.04	0.005	0.0339	CS
18	0.05	0.005	0.0339	D
19	0.06	0.005	0.0339	D
20	0.03	0.005	0.0509	CS
21	0.04	0.005	0.0509	CS
22	0.05	0.005	0.0509	H
23	0.06	0.005	0.0509	D
24	0.07	0.005	0.0509	D
25	0.03	0.005	0.0679	CS
26	0.04	0.005	0.0679	CS
27	0.05	0.005	0.0679	CS
28	0.06	0.005	0.0679	D
29	0.07	0.005	0.0679	D
30	0.04	0.005	0.1019	CS
31	0.05	0.005	0.1019	CS
32	0.06	0.005	0.1019	D
33	0.07	0.005	0.1019	D
34	0.05	0.005	0.1698	CS
35	0.06	0.005	0.1698	H
36	0.08	0.005	0.1698	D
37	0.1	0.005	0.1698	D
38	0.01	0.002	0.2122	CS
39	0.02	0.002	0.2122	CS
40	0.03	0.002	0.2122	CS
41	0.04	0.002	0.2122	H
42	0.05	0.002	0.2122	D
43	0.06	0.002	0.2122	D
44	0.02	0.002	0.1061	CS
45	0.03	0.002	0.1061	CS
46	0.04	0.002	0.1061	D
47	0.05	0.002	0.1061	D
48	0.03	0.002	0.1590	CS
49	0.04	0.002	0.1590	CS
50	0.05	0.002	0.1590	D
51	0.06	0.002	0.1590	D

simulated in our experiments. Potential discrepancies between the values of  $\Pi_6$  in our experiments and geological systems are thus not critical, and  $\Pi_6$  is not considered further in the analysis.

#### 4. Results

Our experimental strategy followed a classical parameter study that consisted of systematically and independently varying the dimensional parameters  $h$ ,  $d$ , and  $v$  (Table 3). Subsequently, we used these dimensional parameters to test the physical effects of the dimensionless numbers identified in the preceding analysis.

The experiments produced two basic sheet intrusion morphologies that compare to natural dikes and cone sheets, as well as a transitional type of intrusion referred to as a hybrid intrusion (Figure 4). The dikes were a few millimeters thick, subvertical, and elliptical (Figure 4a). In most experiments, their tips showed an echelon segmentation. At shallow depths, most dikes split into two moderately dipping branches, producing a rough “boat hull”-shaped intrusion, i.e., an elongated conical morphology, the tip of which pointed downward and was rooted at the tip of the underlying dike; the long axis of this hull-shaped intrusion was parallel to the underlying dike (Figure 4a). The hull-shaped intrusions were similar to the three-dimensional cup-shaped intrusions of *Mathieu et al.* [2008] and the two-dimensional V-shaped intrusions of *Abdelmalak et al.* [2012].

The cone sheets consisted of inclined and curved sheet intrusions a few millimeters thick, exhibiting a conical shape rooted to the injection inlet (Figure 4c). The cones were usually circular to slightly elliptical and varied in upper diameter from 3 to 13 cm. The inner, lower cone geometry varied between steeply to moderately

dipping funnels and rather flat dish shapes. The outer, upper cone geometry exhibited a straight cone shape that flattened upward to form a flat rim close to the surface (i.e., overall trumpet shape).

The hybrid intrusions combined some characteristics of both the experimental dikes and cone sheets (Figure 4b). The detailed shapes varied from one experiment to another. They were commonly characterized by a dike-like lower part directly rooted onto the inlet, whereas the upper part exhibited complex morphologies with several nested cones and offshoots.

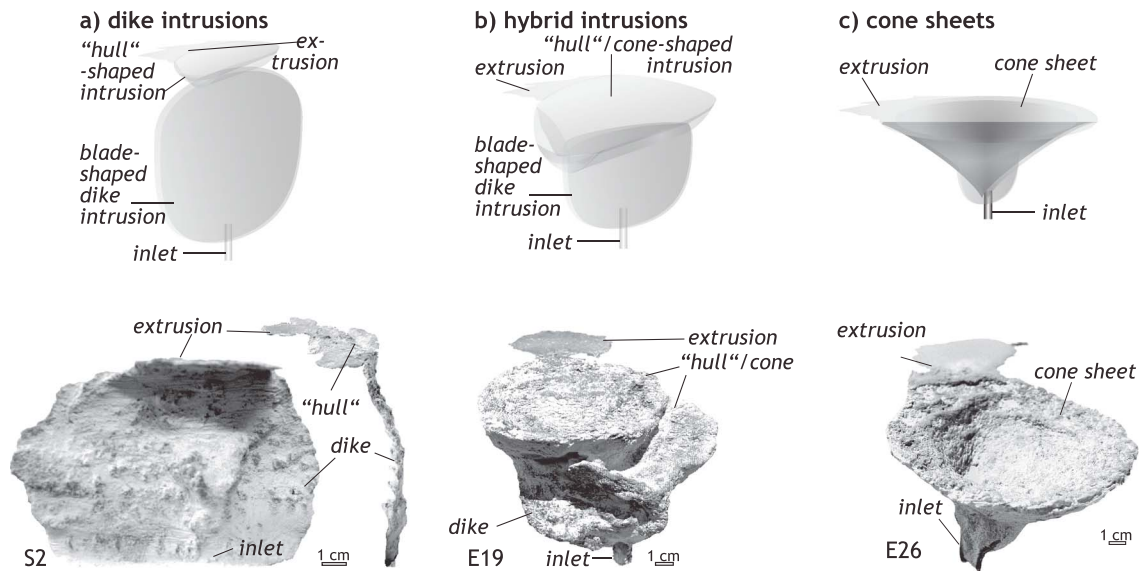


**Figure 4.** (a) Schematic drawing (top) and photograph (bottom) of a typical dike produced during the experiments and excavated from the host powder after solidification of the oil. The dike initiated from the inlet at the bottom and fed an elongated V-shaped, or “hull”-shaped, sheet intrusion to the very top. (b and c) Schematic drawings (top) and photographs (bottom) of typical excavated hybrid and cone sheet intrusions, respectively.

Interpreting experimental results from a parameter study involving several independent variable parameters is challenging. This challenge is here overcome via the dimensional analysis. The advantages of such analysis are to (i) identify the key dimensionless parameters that govern the simulated processes and (ii) display the experimental results in dimensionless plots, such that they can be quantitatively integrated with geological data [see also *Barenblatt, 2003; Galland et al., 2014b*].

Our dimensional analysis identified two main dimensionless parameters that account for coupled effects of the magmatic feeder of dikes or cone sheets and the host rock properties:  $\Pi_1 = h/d$  and  $\Pi_2 = \nu/\rho Cd$ . The depth-to-diameter ratio of the injection inlet,  $\Pi_1$ , is purely geometrical. By comparison, the ratio between the local viscous stresses induced by the oil flow through the inlet and the strength of the flour,  $\Pi_2$ , is dynamical. Plotting the experiments against  $\Pi_1$  and  $\Pi_2$ , we obtain a consistent “phase diagram,” in which the experimental dikes and cone sheets group in a systematic manner into two separate fields (Figure 5). The hybrid intrusions plot along the transition line separating the cone sheet and the dike fields, supporting the idea that they form in a transitional regime. In a log-log plot, this transition is sublinear with a slope  $\alpha = 0.314$ , indicating that it roughly fits a power law of the form  $\Pi_1 \propto \Pi_2^{0.314}$  (Figure 5).

## 5. Interpretation and Discussion

### 5.1. Mechanical Interpretation

The phase diagram in Figure 5 highlights how  $\Pi_1$  and  $\Pi_2$  control the formation of dikes and cone sheets in the models. Importantly, the shape of the modeled intrusion is determined at the very early stages of the experiments, i.e., by the processes at the injection inlet. Transposed to natural volcanic systems, it suggests that dikes preferentially form at high values of  $\Pi_1$ , i.e., when the size (lateral extent) of the magmatic source is small with respect to its depth (Figure 5). Conversely, cone sheets form at relatively low  $\Pi_1$  values, i.e., when the magmatic source is shallow and/or large compared to its depth. Such a result is in good agreement with established conceptual models of cone sheets, which are inferred to result from the interaction between a shallow magma chamber and the free surface [*Anderson, 1936; Phillips, 1974; Bistacchi et al., 2012*].

Figure 5 also shows that dikes preferentially form at low values of  $\Pi_2$ , i.e., when the viscous stresses in the flowing magma are small compared to the strength of the host rock at constant value of  $\Pi_1$  (Figure 5). Conversely, cone sheets preferentially form at higher values of  $\Pi_2$ , i.e., when the viscous stress due to magma flow becomes substantial with respect to the host rock strength. This indicates that cone sheets are expected to form at relatively higher magma influx rates than dikes in volcanic systems. This is again in good agreement

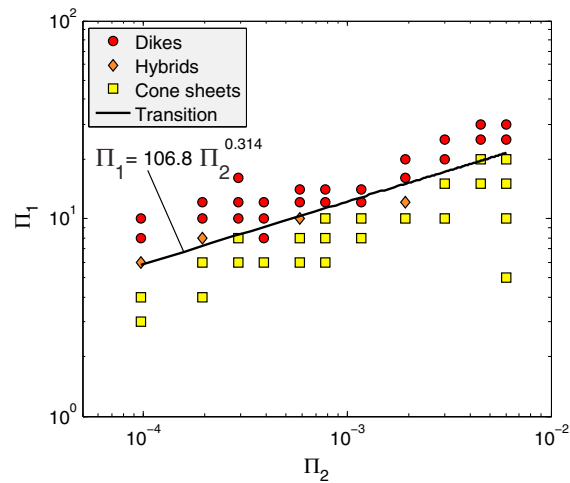


**Figure 5.** Log-log dimensionless phase diagram distinguishing the intrusion shapes obtained in the 51 experiments of this study: dikes (red circles), hybrid intrusions (orange diamonds), and cone sheets (yellow squares). The axes of the diagram give the initial and boundary conditions expressed by the dimensionless parameters  $\Pi_1 = h/d$  and  $\Pi_2 = v\eta/Cd$ . The dikes and cone sheet experiments plot in two distinct fields, separated by a line that is defined by the power law  $\Pi_1 = 106.8 \times \Pi_2^{0.314}$ .

$\eta$  and  $C$  would require additional experiments, in which both  $\eta$  and  $C$  are independently varied in a controlled manner.

A comparison can be made between laboratory models using granular materials and gelatine. Interestingly, gelatine models almost never produce conical intrusions [e.g., *Rivalta and Dahm, 2006; Menand, 2008*], except in the experiments of *McLeod and Tait [1999]*. Our analysis provides elements to explain this observation. Although the cohesion of gelatine has not been measured [*Kavanagh et al., 2013*], gelatine is much stronger than granular materials, such that its cohesion is likely several orders of magnitude higher than those of granular materials. Therefore, the values of  $\Pi_2$  in gelatine experiments are very small, favoring the formation of dikes according to the phase diagram in Figure 5, except when  $\Pi_1$  is small. The latter was the case in the experiments of *McLeod and Tait [1999]*, in which the magmatic source was a shallow large cavity. The formation of cone sheets in most gelatine experiments is therefore unlikely to occur, indicating that gelatine is too strong to simulate natural rocks.

The phase diagram in Figure 5 also explains the transition from dikes to hull-shaped intrusions in most of our experiments. When the injection inlet was deep enough,  $\Pi_1$  was high when the intrusion initiated, leading to a dike. During dike propagation toward the surface, the dike tip acted as a local, moving inlet. The value of  $\Pi_1$  at the dike tip decreased until it crossed the transition between the dike and the cone sheet fields. The hull-shaped intrusions can thus be considered to be cone sheets (or cup-shaped intrusions [*Mathieu et al., 2008*]) sourced from an elongated feeder.

An additional key question concerns the local mechanical processes controlling both the initiation and propagation of either dikes or cone sheets. Figure 5 shows that cone sheets preferentially form at high values of  $\Pi_2$ , i.e., when the viscous stress in the flowing magma is substantial with respect to the strength of the host. In this configuration, the viscous stress in the oil likely modifies the stress in the flour close to the oil/silica flour interface. This may imply that plastic deformation by shearing of the host is substantial in this regime. Such an interpretation is in agreement with the 2-D numerical simulations of *Rozhko et al. [2007]* and the 2-D experiments of *Abdelmalak et al. [2012]* and *Mourgues et al. [2012]*. These authors show that dikes propagate as viscous indenters, as also suggested by *Mathieu et al. [2008]*. When a dike tip becomes shallow, it interacts with shear fractures that lead to the splitting of the dike tip into two branches. Following *Abdelmalak et al. [2012]* and *Mourgues et al. [2012]*, we infer that open (mode I) fracturing might control the intrusion mechanism in the dike field of Figure 5, as commonly indicated in the literature [e.g., *Pollard, 1987; Lister and*

with geological observations, for instance at the Miocene Otoge igneous complex, Central Japan, where the emplacement of cone sheets is inferred to result from high magma supply rate, whereas the emplacement of dikes is inferred to result from a decrease of magma supply rate [*Geshi, 2005*]. The phase diagram of Figure 5 also shows that at constant  $\Pi_1$ , i.e., for a single magma source, both dikes and cone sheets may form depending on the value of  $\Pi_2$ .

Note that  $\Pi_2$  includes the viscosity ( $\eta$ ) of the intruding fluid and the cohesion ( $C$ ) of the intruded material, quantities that were kept constant in our experimental series. However, the dimensional analysis indicates that the physically meaningful parameter is  $\Pi_2$ , not the individual dimensional parameters considered independently [*Barenblatt, 2003; Galland et al., 2014b*]. Therefore, it is relevant to account for  $\eta$  and  $C$  in the phase diagram of Figure 5, and our interpretation of the results is only based on  $\Pi_1$  and  $\Pi_2$ . Testing the effects of

Kerr, 1991; Rubin, 1995], whereas shear failure (mode II fracturing) might control the initiation of the intrusion, and possibly its subsequent propagation, in the cone sheet field [Rozhko et al., 2007]. This interpretation is in agreement with the conclusions of Phillips [1974]. It is also corroborated by the experimental results of Galland [2012], who show that cone sheets result in a smooth subcircular uplifted area at the surface, the eruption occurring at the edge of the uplifted area, i.e., where the shear stresses are at a maximum. This interpretation also indicates that purely elastic models, commonly used to analyze the emplacement of dikes and cone sheets, are probably too simple.

The initiation of cone sheets by shear failure seemingly contradicts some field observations in cone sheet swarms where no relative displacement of host rock markers along sheet walls has been found, suggesting that they propagate as mode I fractures [e.g., Klausen, 2006; Burchardt and Gudmundsson, 2009; Siler and Karson, 2009; Tibaldi et al., 2011]. However, initial shear failure of any material does not imply a finite displacement of the fracture walls, since even joints, i.e., fractures without relative displacement of their walls, may be initiated by shear failure [e.g., Engelder, 1987; Davis and Reynolds, 1996]. Our results and interpretation of the experiments thus suggest that magma injection, deformation of the host rocks, and opening of the propagating cone sheet fracture could obliterate any signs of initial shear failure, in nature.

Mathieu et al. [2008] observed the transition from vertical dike to cup-shaped intrusion at shallow depth. They attempted to analyze the mechanisms controlling such transition, but their dimensional analysis is flawed for several reasons. (i) They correlated dimensionless parameters that combine both output and input parameters (their Figure 5c). In this figure, the observed correlation just illustrates that the dip angles of their cup-shaped intrusions are constant. (ii) They defined the dimensionless parameters using the total height of their models, which is meaningless and cannot be constrained in nature. (iii) Their dimensionless number " $\Pi_4$  (viscosity)" has no physical meaning, and so no physical relevance, explaining the poor correlation in their Figure 5b. In contrast, the consistency of our experimental results in Figure 5 and the physical meaning of the dimensionless numbers defined in our analysis demonstrate that (i) the empirical law identified in the phase diagram is physically relevant and (ii) we have constrained and related two physical dynamic regimes of magma emplacement.

## 5.2. Geological Implications

A critical issue in our models concerns the geological relevance of the injection inlet, and especially the meaning of the lateral extent  $d$  used to calculate  $\Pi_1$  and  $\Pi_2$ . One could argue that our inlet is not representative of, e.g., the roof of a large sill or of a wide magma reservoir. Actually, our experimental procedure is not designed to simulate magmatic systems of given sizes and shapes, but to identify general, dimensionless, mechanical laws governing the emplacement of magma in the Earth's crust. The law identified with our results is the power law controlling the transition between the dike and the cone sheet emplacement regimes (Figure 5). In the following, we discuss the applicability of our empirical law to various magmatic settings.

The ranges of  $\Pi_1$  and  $\Pi_2$  only cover 2 orders of magnitude (Figure 5). This narrow range cannot account for the wide ranges of  $\Pi_1$  and  $\Pi_2$  in geological systems, as shown in Figure 6. However, if the empirical law identified in Figure 5 is a general physical law governing magma emplacement in the Earth's crust, it must be valid across larger ranges of  $\Pi_1$  and  $\Pi_2$ . To test the relevance of our empirical law, we extrapolate it over the geological ranges of  $\Pi_1$  and  $\Pi_2$ , and compare it with magmatic feeders of dikes and cone sheets of different scales and shapes (Figure 6).

In Figure 6, we consider three main types of magmatic feeders leading to dikes and/or cone sheets: (i) sills in sedimentary basins dominantly leading to the formation of subcircular inward dipping inclined sheets (Figures 1e and 1f [Malthe-Sørenssen et al., 2004; Galland et al., 2009; Galland and Scheibert, 2013]); (ii) dike tips, considered as local moving magma sources, which dominantly propagate as dikes or sometimes split into V-shaped, hull-shaped, or cup-shaped intrusions (Figure 1d [Mathieu et al., 2008; Abdelmalak et al., 2012; Galland, 2012; Mourgues et al., 2012]); (iii) magmatic reservoirs beneath central volcanoes, which feed both dikes and cone sheets (Figure 1a). If the empirical law of Figure 5 is valid for the general processes of magma emplacement in the Earth's crust, it should predict that the values of  $\Pi_1$  and  $\Pi_2$  for sills plot dominantly in the cone sheet field, dike tips plot dominantly in the dike field, and magma reservoirs plot on the transition between the dike and cone sheet fields. Estimating the exact values of  $\Pi_1$  and  $\Pi_2$  in magma reservoirs, sills, and dike tips, however, is challenging, as (i) natural host rocks are heterogeneous and exhibit contrasting

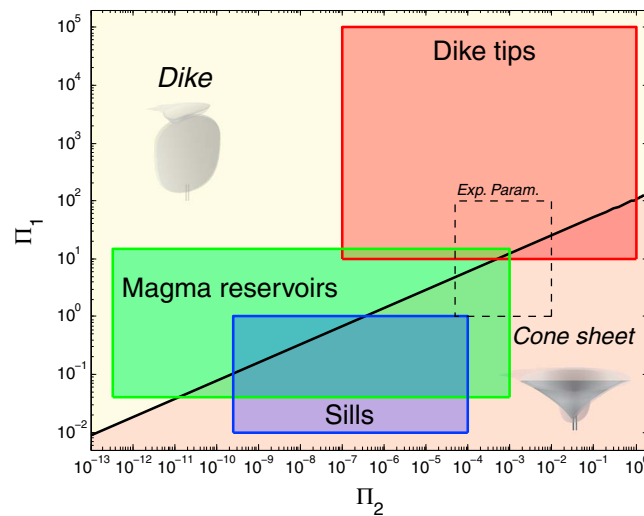


**Figure 6.** Graph comparing the experimental results of this study (dashed box) to characteristic geological values of  $\Pi_1$  and  $\Pi_2$ . The dike-to-cone sheet transition is extrapolated from the phase diagram of Figure 5. Geological boxes correspond to dike tips (red), magma reservoirs in volcanoes (green), and shallow sills in sedimentary basins (blue). See Table 1 for natural values of  $\Pi_1$  and  $\Pi_2$ .

Sills mostly plot in the cone sheet regime (Figure 6), which is also in very good agreement with geological observations and our current understanding of the way they form. Indeed, inclined sheets of saucer-shaped sills can be regarded as cone

sheets fed from flat, shallow sills [Malthe-Sørenssen et al., 2004; Galland et al., 2009; Galland and Scheibert, 2013]. Exceptions are expected from the upper left corner of the saucer-shaped sill box that plots in the dike field, and which corresponds to deep sills fed by low-viscosity magmas at low influx rates and intruding very stiff rocks. Typical dike tips mostly fall into the dike field, as expected. This indicates that dikes represent stable intrusions that are unlikely to split and form cone sheets. Nevertheless, very shallow dikes filled with viscous magma or intruding weak rocks (lower right corner of the red field in Figure 6) might split to form cone sheets (see field example in Figure 1d).

The magma reservoir field plots on both sides of the dike-to-cone sheet transition (Figure 6), predicting that both dikes and cone sheets can form and coexist in the same volcanic systems, as observed in the field, and may be fed by the same reservoir [Walker, 1992; Ancochea et al., 2003; Geshi, 2005; Burchardt et al., 2011]. According to our experimental results, this implies that temporal changes in the dynamics of a single source (i.e.,  $\Pi_2$  variations, possibly due to influx rate changes), or, alternatively, different magmatic sources (i.e.,  $\Pi_1$  variations, implying sources of different sizes and/or depths), were involved from one type of intrusion to the other at volcanoes exhibiting both dikes and cone sheets [e.g., Gudmundsson, 1998; Ancochea et al., 2003; Geshi, 2005]. Note that the magma reservoir field plots in the dike field to a greater extent than in the cone sheet field, suggesting that dikes are more likely to form than cone sheets in volcanic systems. This is also corroborated by geological observations, as dikes are usually more common than cone sheets [e.g., Nakamura, 1977; Smith, 1987; Ernst et al., 1995; Paquet et al., 2007].

Most numerical models consider a simple pressure buildup inside a magma source of given shape, until the stresses in the elastic host rock locally exceed a rupture limit [e.g., Bistacchi et al., 2012; Chestler and Grosfils, 2013]. Depending on the orientation of the principal stresses at the rupture point, the formation of a dike, or a cone sheet, is inferred. Nevertheless, for given magmatic reservoir shape, depth, and size, the stress orientation at the rupture limit will always be the same, so elastic models considering fixed reservoirs cannot explain how a single magmatic source may lead to both dikes and cone sheets. In contrast, our laboratory models show that for a given magmatic source shape (constant  $\Pi_1$ ), variable values of  $\Pi_2$  lead either to the formation of dikes or cone sheets. Therefore, our results indicate that (i) elastic models do not fully address the mechanics of dike and cone sheet emplacement, and (ii) the dynamics of the viscous magma also needs to be considered.

Figure 6 shows that there is a good match between our laboratory results and geological data. Nevertheless, the ranges of geological values of  $\Pi_1$  and  $\Pi_2$  for different magmatic sources are only rough estimates given as orders of magnitude, due to the large uncertainties attached to the natural values of, e.g.,  $v$ ,  $\eta$ , and  $C$ .

cohesions [Schellart, 2000], (ii) magma viscosity is variable, mostly depending on chemical composition [Dingwell et al., 1993], (iii) the depth and lateral extents of magma sources are difficult to constrain precisely, and (iv) the exact values of the magma velocities, especially within sills and magma reservoirs, are poorly constrained. Therefore, the analysis is based on estimates of  $\Pi_1$  and  $\Pi_2$  orders of magnitude. The ranges of  $\Pi_1$  and  $\Pi_2$  for the three types of magmatic feeders are plotted as colored fields in Figure 6.

Consequently, we expect the real geological ranges of  $\Pi_1$  and  $\Pi_2$  to be smaller than those shown by the boxes in Figure 6, so that the natural sill and dike boxes are probably more restricted within the respective sill and dike fields, which strengthens our conclusions.

According to the principle of similarity developed by *Hubbert [1937]*, *Ramberg [1981]*, and *Barenblatt [2003]*, our experiments are not, strictly speaking, simulating the three magmatic feeding systems discussed in Figure 6. For example, considering the scale ratio between our models and the natural systems, our 2 mm dikes theoretically simulate 20 to 200 m thick dikes, which are very thick compared to usual dikes. Nevertheless, the aim of our experimental series was not to mimic specifically one or another intrusion type, but instead to identify the general mechanical law governing the transition between the emplacement regimes leading to either dikes or cone sheets. For this purpose, we have chosen experimental parameters that cover a range appropriate to identify this law. The excellent match between our extrapolated empirical power law with geological data from magmatic feeding systems of various sizes and shapes confirms a posteriori that the experimental results can be applied to a wide range of scales. Therefore, this law expresses a fundamental general process of magma emplacement in the brittle crust that unifies magmatic systems of different scales and geological settings.

Our experiments, however, do not account for regional tectonic stresses and topography, which are known to influence the emplacement of dikes and cone sheets [e.g., *Chadwick and Dieterich, 1995*; *Kervyn et al., 2009*]. In addition, our injection inlet is circular, whereas some elliptical magma reservoirs [e.g., *Burchardt et al., 2013*] and sills [e.g., *Galerne et al., 2011*] have been documented. Regional tectonics, topography, and the shape of the source are expected to affect the dike-to-cone sheet transition. Nevertheless, the good match between our extrapolated empirical results and geological data from various volcanic settings (Figure 6) suggests that the empirical law separating the dike field from the cone sheet field can be applied over 4 orders of magnitude with respect to  $\Pi_1$  and 13 orders of magnitude with respect to  $\Pi_2$ . In comparison, the stresses in the Earth's crust affected by regional tectonics and topography remain on the same orders of magnitude. We infer that stresses due to regional tectonics and topography therefore only slightly change the position or the slope of the dike-to-cone sheet transition in our phase diagram in Figures 5 and 6, but the first-order trend identified in our experiments would remain. To quantify how tectonic stresses and topography affect the dike-to-cone sheet transition, more experiments are required.

## 6. Conclusions

This contribution describes the results of 51 laboratory models of magma emplacement in the brittle crust. We performed a parameter study, in which we varied systematically the depth of the injection inlet, its thickness, and the injection velocity. The main results of our study are the following:

1. Our models dynamically simulate vertical dikes, cone sheets, and hybrid intrusions exhibiting characteristics of both dikes and cone sheets.
2. We performed a dimensional analysis of the simulated processes and identified two main dimensionless parameters governing the emplacement of magma in the brittle crust: a geometric parameter  $\Pi_1$  accounting for the depth-to-lateral extent of the magmatic source, and a dynamic parameter  $\Pi_2$  accounting for the ratio between the local viscous stresses and the cohesion of the host rock.
3. Plotting  $\Pi_1$  against  $\Pi_2$  for the experiments, we obtain a consistent dimensionless phase diagram, in which the experimental dikes and cone sheets group in a systematic manner into two separate fields.
4. The hybrid intrusions plot along the transition line separating the cone sheet and the dike fields, supporting the idea that they form in a transitional regime. The dike-to-cone sheet transition is sharp and roughly fits a power law of the form  $\Pi_1 \propto \Pi_2^{0.314}$ .
5. The comparison between our experimental results and geological data from various magmatic feeding systems suggests that our empirical dike-to-cone sheet power law transition can be extrapolated to a wide range of magmatic settings. This indicates that our experimental models capture general magma emplacement mechanisms, reconciling existing specific models of distinct magmatic feeding systems.

## References

- Abdelmalak, M. M., R. Mourgues, O. Galland, and D. Bureau (2012), Fracture mode analysis and related surface deformation during dyke intrusion: Results from 2D experimental modelling, *Earth Planet. Sci. Lett.*, 359–360, 93–105, doi:10.1016/j.epsl.2012.10.008.

### Acknowledgments

The authors acknowledge constructive discussions with L. Mathieu. This study was supported by a Center of Excellence grant from the Norwegian Research Council to PGP (grant 146031). The experimental apparatus was machined by the technical staff of the Physics Department of the University of Oslo and benefited from the technical expertise of the electronic engineer at PGP, O. Gundersen. S.B. acknowledges financial support from V.R. Troll, Uppsala University, and the Swedish Research Council. E.H. acknowledges his welcome to PGP for several weeks thanks to a half-year sabbatical, teaching-free CRCT from Université de Rennes 1. C.B. acknowledges an Aurora grant 221616 for his research visit in Oslo. The data used in this paper are available from the authors. We acknowledge the very constructive reviews by N. Geshi, J. Ruch, and Associate Editor M. Poland.

- Amelung, F., S. Jonsson, H. Zebker, and P. Segall (2000), Widespread uplift and "trapdoor" faulting on Galápagos volcanoes observed with radar interferometry, *Nature*, *407*(6807), 993–996, doi:10.1038/35039604.
- Ancochea, E., M. J. Huertas, F. Hernán, and J. L. Brändle (2014), A new felsic cone-sheet swarm in the Central Atlantic Islands: The cone-sheet swarm of Boa Vista (Cape Verde), *J. Volcanol. Geotherm. Res.*, *274*, 1–15, doi:10.1016/j.jvolgeores.2014.01.010.
- Ancochea, E., J. L. Brändle, M. J. Huertas, C. R. Cubas, and F. Hernan (2003), The felsic dikes of La Gomera (Canary Islands): Identification of cone sheet and radial dike swarms, *J. Volcanol. Geotherm. Res.*, *120*(3–4), 197–206.
- Anderson, E. M. (1936), The dynamics of the formation of cone sheets, ring dykes and cauldron subsidences, *Proc. R. Soc. Edin.*, *56*, 128–163.
- Bailey, S. E. B. (1924), Tertiary and post-Tertiary geology of Mull, Loch Aline, and Oban: A description of parts of sheets 43, 44, 51, and 52 of the geological map, HMSO.
- Barenblatt, G. I. (2003), *Scaling*, 171 pp., Cambridge Univ. Press, Cambridge, U. K.
- Bistacchi, A., A. Tibaldi, F. A. Pasquaré, and D. Rust (2012), The association of cone-sheets and radial dykes: Data from the Isle of Skye (UK), numerical modelling, and implications for shallow magma chambers, *Earth Planet. Sci. Lett.*, *339–340*, 46–56, doi:10.1016/j.epsl.2012.05.020.
- Burchardt, S. (2008), New insights into the mechanics of sill emplacement provided by field observations of the Njardvik Sill, Northeast Iceland, *J. Volcanol. Geotherm. Res.*, *173*(3–4), 280–288, doi:10.1016/j.jvolgeores.2008.02.009.
- Burchardt, S., and A. Gudmundsson (2009), The infrastructure of Geitafell volcano, southeast Iceland, in *Studies in Volcanology: The Legacy of George Walker, Spec. Publ. of IAVCEI*, vol. 2, edited by T. Thordarson et al., pp. 349–370, Geological Society, London, U. K.
- Burchardt, S., D. C. Tanner, V. R. Troll, M. Krumbholz, and L. E. Gustafsson (2011), Three-dimensional geometry of concentric intrusive sheet swarms in the Geitafell and the Dyrhöll volcanoes, eastern Iceland, *Geochem. Geophys. Geosyst.*, *12*, QA0B09, doi:10.1029/2011gc003527.
- Burchardt, S., V. R. Troll, L. Mathieu, H. C. Emeleus, and C. H. Donaldson (2013), Ardnamurchan 3D cone-sheet architecture explained by a single elongate magma chamber, *Sci. Rep.*, *3*, doi:10.1038/srep02891.
- Bureau, D., R. Mourgues, J. Cartwright, M. Foschi, and M. M. Abdelmalak (2013), Characterisation of interactions between a pre-existing polygonal fault system and sandstone intrusions and the determination of paleo-stresses in the Faroe-Shetland basin, *J. Struct. Geol.*, *46*, 186–199, doi:10.1016/j.jsg.2012.09.003.
- Chadwick, W. W. J., and J. H. Dieterich (1995), Mechanical modeling of circumferential and radial dike intrusion on Galápagos volcanoes, *J. Volcanol. Geotherm. Res.*, *66*, 37–52.
- Chadwick, W. W. J., S. Jonsson, D. J. Geist, M. Poland, D. J. Johnson, S. Batt, K. S. Harpp, and A. Ruiz (2011), The May 2005 eruption of Fernandina volcano, Galápagos: The first circumferential dike intrusion observed by GPS and InSAR, *Bull. Volcanol.*, *73*(6), 679–697, doi:10.1007/s00445-010-0433-0.
- Chestler, S. R., and E. B. Grosfils (2013), Using numerical modeling to explore the origin of intrusion patterns on Fernandina volcano, Galápagos Islands, Ecuador, *Geophys. Res. Lett.*, *40*, 4565–4569, doi:10.1002/grl.50833.
- Davis, G. H., and S. J. Reynolds (1996), *Structural Geology of Rocks and Regions*, 2nd ed., John Wiley, New York.
- Dingwell, D. B., N. S. Bagdassarov, G. Y. Bussov, and S. L. Webb (1993), Magma rheology, in *Experiments at High Pressure and Applications to the Earth's Mantle, Short Course Handbook*, 21, edited by R. W. Luth, pp. 131–196, Mineralogists Association of Canada, Edmonton, Alta., Canada.
- Engelder, T. (1987), Joints and shear fractures in rock, in *Fracture Mechanics of Rock*, edited by B. K. Atkinson, pp. 27–69, Academic Press, London, U. K.
- Ernst, R. E., J. W. Head, E. Parfitt, E. Grosfils, and L. Wilson (1995), Giant radiating dyke swarms on Earth and Venus, *Earth Sci. Rev.*, *39*, 1–58.
- Galerne, C. Y., E. R. Neumann, and S. Planke (2008), Emplacement mechanisms of sill complexes: Information from the geochemical architecture of the Golden Valley Sill Complex, South Africa, *J. Volcanol. Geotherm. Res.*, *177*(2), 425–440.
- Galerne, C. Y., O. Galland, E. R. Neumann, and S. Planke (2011), 3D relationships between sills and their feeders: Evidence from the Golden Valley Sill Complex (Karoo Basin) and experimental modelling, *J. Volcanol. Geotherm. Res.*, *202*(3–4), 189–199, doi:10.1016/j.jvolgeores.2011.02.006.
- Galland, O. (2012), Experimental modelling of ground deformation associated with shallow magma intrusions, *Earth Planet. Sci. Lett.*, *317–318*, 145–156, doi:10.1016/j.epsl.2011.10.017.
- Galland, O., and J. Scheibert (2013), Analytical model of surface uplift above axisymmetric flat-lying magma intrusions: Implications for sill emplacement and geodesy, *J. Volcanol. Geotherm. Res.*, *253*, 114–130, doi:10.1016/j.jvolgeores.2012.12.006.
- Galland, O., P. R. Cobbold, E. Hallot, J. de Bremond d'Ars, and G. Delavaud (2006), Use of vegetable oil and silica powder for scale modelling of magmatic intrusion in a deforming brittle crust, *Earth Planet. Sci. Lett.*, *243*, 786–804.
- Galland, O., P. R. Cobbold, J. de Bremond d'Ars, and E. Hallot (2007), Rise and emplacement of magma during horizontal shortening of the brittle crust: Insights from experimental modeling, *J. Geophys. Res.*, *112*, B06402, doi:10.1029/2006JB004604.
- Galland, O., S. Planke, E. R. Neumann, and A. Malthe-Sørenssen (2009), Experimental modelling of shallow magma emplacement: Application to saucer-shaped intrusions, *Earth Planet. Sci. Lett.*, *277*(3–4), 373–383.
- Galland, O., G. R. Gisler, and Ø. T. Haug (2014a), Morphology and dynamics of explosive vents through cohesive rock formations, *J. Geophys. Res. Solid Earth*, *119*, 4708–4728, doi:10.1002/2014JB011050.
- Galland, O., E. P. Holohan, and G. Dumazer (2014b), The use of scaling theory in geological laboratory models, *GeoMod 2014*, GFZ Potsdam, Germany, 31 August - 5 September.
- Geshi, N. (2005), Structural development of dike swarms controlled by the change of magma supply rate: The cone sheets and parallel dike swarms of the Miocene Otoge igneous complex, Central Japan, *J. Volcanol. Geotherm. Res.*, *141*(3–4), 267–281, doi:10.1016/j.jvolgeores.2004.11.002.
- Gudmundsson, A. (1998), Magma chambers modeled as cavities explain the formation of rift zone central volcanoes and their eruption and intrusion statistics, *J. Geophys. Res.*, *103*(B4), 7401–7412, doi:10.1029/97JB03747.
- Harker, A., and C. T. Clough (1904), *The Tertiary Igneous Rocks of Skye, Mem. Geol. Surv. Scotl.*
- Hubbert, M. K. (1937), Theory of scale models as applied to the study of geologic structures, *Geol. Soc. Am. Bull.*, *48*, 1459–1520.
- Hubbert, M. K. (1951), Mechanical basis for certain familiar geologic structures, *Geol. Soc. Am. Bull.*, *62*, 355–372.
- Huppert, H., and R. S. Sparks (1981), The fluid dynamics of a basaltic magma chamber replenished by influx of hot, dense ultrabasic magma, *Contrib. Mineral. Petrol.*, *75*(3), 279–289, doi:10.1007/bf01166768.
- Kavanagh, J. L., T. Menand, and R. S. J. Sparks (2006), An experimental investigation of sill formation and propagation in layered elastic media, *Earth Planet. Sci. Lett.*, *245*(3–4), 799–813.
- Kavanagh, J. L., T. Menand, and K. A. Daniels (2013), Gelatine as a crustal analogue: Determining elastic properties for modelling magmatic intrusions, *Tectonophysics*, *582*, 101–111, doi:10.1016/j.tecto.2012.09.032.
- Kervyn, M., G. G. J. Ernst, B. van Wyk de Vries, L. Mathieu, and P. Jacobs (2009), Volcano load control on dyke propagation and vent distribution: Insights from analogue modeling, *J. Geophys. Res.*, *114*, B03401, doi:10.1029/2008jb005653.
- Klausen, M. B. (2004), Geometry and mode of emplacement of the Thverartindur cone sheet swarm, SE Iceland, *J. Volcanol. Geotherm. Res.*, *138*(3–4), 185–204.

- Klausen, M. B. (2006), Geometry and mode of emplacement of dike swarms around the Birnadalstindur igneous centre, SE Iceland, *J. Volcanol. Geotherm. Res.*, *151*(4), 340–356.
- Krumbholz, M., C. F. Hieronymus, S. Burchardt, V. R. Troll, D. C. Tanner, and N. Friese (2014), Weibull-distributed dyke thickness reflects probabilistic character of host-rock strength, *Nat. Commun.*, *5*, doi:10.1038/ncomms4272.
- Lister, J. R., and R. C. Kerr (1991), Fluid-mechanical models of crack propagation and their application to magma transport in dykes, *J. Geophys. Res.*, *96*(B6), 10,049–10,077, doi:10.1029/91JB00600.
- Malthe-Sørenssen, A., S. Planke, H. Svensen, and B. Jamtveit (2004), Formation of saucer-shaped sills, in *Physical Geology of High-Level Magmatic Systems*, edited by C. Breitkreuz and N. Petford, *Geol. Soc. London Spec. Publ.*, *234*, pp. 215–227.
- Mathieu, L., B. van Wyk de Vries, E. P. Holohan, and V. R. Troll (2008), Dykes, cups, saucers and sills: Analogue experiments on magma intrusion into brittle rocks, *Earth Planet. Sci. Lett.*, *271*(1–4), 1–13.
- McLeod, P., and S. Tait (1999), The growth of dykes from magma chambers, *J. Volcanol. Geotherm. Res.*, *92*, 231–245.
- Menand, T. (2008), The mechanics and dynamics of sills in layered elastic rocks and their implications for the growth of laccoliths and other igneous complexes, *Earth Planet. Sci. Lett.*, *267*(1–2), 93–99.
- Menand, T., and S. Tait (2001), A phenomenological model for precursor volcanic eruptions, *Nature*, *411*, 678–680.
- Menand, T., and S. Tait (2002), The propagation of a buoyant liquid-filled fissure from a source under constant pressure: An experimental approach, *J. Geophys. Res.*, *107*(B11), 2306, doi:10.1029/2001JB000589.
- Merle, O., and A. Borgia (1996), Scaled experiments of volcanic spreading, *J. Geophys. Res.*, *101*(B6), 13,805–13,817, doi:10.1029/95JB03736.
- Mourgues, R., and P. R. Cobbold (2003), Some tectonic consequences of fluid overpressures and seepage forces as demonstrated by sandbox modelling, *Tectonophysics*, *376*, 75–97.
- Mourgues, R., D. Bureau, L. Bodet, A. Gay, and J. B. Gressier (2012), Formation of conical fractures in sedimentary basins: Experiments involving pore fluids and implications for sandstone intrusion mechanisms, *Earth Planet. Sci. Lett.*, *313–314*, 67–78, doi:10.1016/j.epsl.2011.10.029.
- Nakamura, K. (1977), Volcanoes as possible indicators of tectonic stress orientation—principle and proposal, *J. Volcanol. Geotherm. Res.*, *2*(1), 1–16.
- Paquet, F., O. Dauteuil, E. Hallot, and F. Moreau (2007), Tectonics and magma dynamics coupling in a dyke swarm of Iceland, *J. Struct. Geol.*, *29*(9), 1477–1493, doi:10.1016/j.jsg.2007.06.001.
- Phillips, W. J. (1974), The dynamic emplacement of cone sheets, *Tectonophysics*, *24*, 69–84.
- Pollard, D. D. (1987), Elementary fracture mechanics applied to the structural interpretation of dikes, in *Mafic Dyke Swarms*, edited by H. C. Halls and W. F. Fahrig, *Geol. Assoc. Can. Spec. Pap.*, *34*, pp. 5–24.
- Polteau, S., E. C. Ferré, S. Planke, E.-R. Neumann, and L. Chevallier (2008a), How are saucer-shaped sills emplaced? Constraints from the Golden Valley Sill, South Africa, *J. Geophys. Res.*, *113*, B12104, doi:10.1029/2008JB005620.
- Polteau, S., A. Mazzini, O. Galland, S. Planke, and A. Malthe-Sørenssen (2008b), Saucer-shaped intrusions: Occurrences, emplacement and implications, *Earth Planet. Sci. Lett.*, *266*(1–2), 195–204.
- Ramberg, H. (1981), *Gravity, Deformation and the Earth's Crust*, 452 pp., Academic Press, New York.
- Rivalta, E., and T. Dahm (2006), Acceleration of buoyancy-driven fractures and magmatic dikes beneath the free surface, *Geophys. J. Int.*, *166*(3), 1424–1439, doi:10.1111/j.1365-246X.2006.02962.x.
- Rozhko, A. Y., Y. Y. Podladchikov, and F. Renard (2007), Failure patterns caused by localization rise in pore-fluid overpressure and effective strength of rocks, *Geophys. Res. Lett.*, *34*, L22304, doi:10.1029/2007GL031696.
- Rubin, A. M. (1995), Propagation of magma-filled cracks, *Annu. Rev. Earth Planet. Sci.*, *23*, 287–336.
- Schellart, W. P. (2000), Shear test results for cohesion and friction coefficients for different materials: Scaling implications for their usage in analogue modelling, *Tectonophysics*, *324*, 1–16.
- Schirnick, C., P. van den Bogaard, and H.-U. Schmincke (1999), Cone sheet formation and intrusive growth of an oceanic island: The Miocene Tejada complex on Gran Canaria (Canary Islands), *Geology*, *27*(3), 207–210, doi:10.1130/0091-7613(1999)027<0207:csfaig>2.3.co;2.
- Sigmundsson, F., et al. (2010), Intrusion triggering of the 2010 Eyjafjallajökull explosive eruption, *Nature*, *468*(7322), 426–430, doi:10.1038/nature09558.
- Siler, D. L., and J. A. Karson (2009), Three-dimensional structure of inclined sheet swarms: Implications for crustal thickening and subsidence in the volcanic rift zones of Iceland, *J. Volcanol. Geotherm. Res.*, *188*(4), 333–346.
- Smith, R. P. (1987), Dyke emplacement at Spanish Peaks, Colorado, in *Mafic Dyke Swarms*, edited by H. C. Halls and W. F. Fahrig, *Geol. Assoc. Can. Spec. Pap.*, *34*, pp. 47–54.
- Sparks, R. S. J., H. E. Huppert, J. S. Turner, M. Sakuyama, and M. J. O'Hara (1984), The fluid dynamics of evolving magma chambers [and discussion], *Philos. Trans. R. Soc. London, Ser. A*, *310*, 511–534.
- Takada, A. (1990), Experimental study on propagation of liquid-filled crack in gelatin: Shape and velocity in hydrostatic stress condition, *J. Geophys. Res.*, *95*(B6), 8471–8481, doi:10.1029/JB095iB06p08471.
- Tibaldi, A., A. F. Pasquaré, and D. Rust (2011), New insights into the cone sheet structure of the Cuillin Complex, Isle of Skye, Scotland, *J. Geol. Soc. London*, *168*(3), 689–704, doi:10.1144/0016-76492009-175.
- Walker, G. P. L. (1992), Coherent intrusion complexes" in large basaltic volcanoes: A new structural model, *J. Volcanol. Geotherm. Res.*, *50*(1–2), 41–54, doi:10.1016/0377-0273(92)90036-D.